Applied Catalysis B: Environmental 142–143 (2013) 761–768

Contents lists available at SciVerse ScienceDirect

Applied Catalysis B: Environmental

journal homepage: www.elsevier.com/locate/apcatb

Tuning the photocatalytic selectivity of TiO_2 anatase nanoplates by altering the exposed crystal facets content

Maria-Veronica Sofianou[a], Vassilis Psycharis[a], Nikos Boukos[a], Tiverios Vaimakis[b], Jiaguo Yu[c], Ralf Dillert[d], Detlef Bahnemann[c], Christos Trapalis[a,*]

[a] Institute of Advanced Materials, Physicochemical Processes, Nanotechnology and Microsystems, NCSR Demokritos, 153 10, Ag. Paraskevi, Attikis, Greece
[b] Department of Chemistry, University of Ioannina, 451 10 Ioannina, Greece
[c] State Key Laboratory for Advanced Technology Materials Synthesis & Processing, Wuhan University of Technology, Wuhan 430070, People's Republic of China
[d] Institut fuer Technische Chemie, Leibniz Universitaet Hannover, Callinstrasse 3, D-30167 Hannover, Germany

ARTICLE INFO

Article history:
Received 21 January 2013
Received in revised form 6 June 2013
Accepted 12 June 2013
Available online 22 June 2013

Keywords:
TiO_2 nanoplates
{1 0 1} {0 0 1} facets
Photoctalysis
NO oxidation
Acetaldehyde decomposition

ABSTRACT

TiO_2 anatase nanoplates were fabricated by a solvothermal method using titanium isopropoxide as a titanium precursor and HF as a capping agent in order to enhance the formation of the {0 0 1} crystal facets of the anatase crystal. Two different surface modification procedures were applied in order to remove the adsorbed fluoride anions on the {0 0 1} crystal facets of the nanoplates. The first procedure was by calcining the as-prepared TiO_2 anatase nanoplates up to 600 °C and the second one was by washing them with a NaOH aqueous solution. Importantly, the surface modification procedure leads to the formation of two different morphologies of the TiO_2 anatase nanoplates which exhibited tunable photocatalytic selectivity in air pollutants purification. The calcined nanoplates became larger and their {1 0 1} crystal facets expanded by shrinking the {0 0 1} crystal facets. In contrast the washed nanoplates maintained their shape which was formed by the solvothermal method. All samples that were calcined or washed, exhibited high photonic efficiency for air pollutants oxidation. The calcined TiO_2 anatase nanoplates exhibited the best photocatalytic activity in oxidizing the NO gas to NO_2 and NO_3^- whereas the washed TiO_2 anatase nanoplates, preserving the initial morphology, exhibited the best photocatalytic activity in decomposing acetaldehyde. The dominant exposed {1 0 1} or {0 0 1} crystal facets of the TiO_2 anatase nanoplates is the key factor in tuning the adsorption selectivity of the air pollutants.

1. Introduction

Over the last years air pollution has been an issue that concerns diverse scientific fields due to the major side-effects that are caused to the natural and built environment as well as to humans and to every other living organism [1–3]. Nitrogen oxides (NO_x) and volatile organic compounds (VOCs) are listed as major primary pollutants whose combinations produce secondary pollutants such as ground level ozone and peroxyacetyl nitrate [4–6]. A potentially promising approach towards solving these environmental issues that are directly connected to the previously mentioned air pollutants is using the titanium dioxide (TiO_2) semiconductor for heteregenous photocatalytic oxidation [7–9].

The anatase phase of the TiO_2 has in most cases higher photocatalytic activity in comparison to the rutile and brookite phase, which are the other crystalline allotropies [10–12]. In general, photocatalysis occurs when a photocatalyst is exposed to photons with at least, as much energy as the band gap of the photocatalyst. Absorption of a photon by a photocatalyst creates electron–hole (e^-/h^+) pairs, which lead to either recombination or undergo subsequent redox reactions by surface radicals, like superoxide ions (O^{2-}) and hydroxyl radicals (OH^-) [13–15]. The photocatalytic activity of the photocatalyst clearly depends on the recombination rate of the electron and hole. This implies that a low recombination rate will significantly enhance the photocatalytic properties of the photocatalyst.

Recently, several studies have shown that the reduction and oxidation sites on the surface of the anatase TiO_2 single crystals are spatially separated because of the selective migration of excited electrons on the {1 0 1} crystal facets and positive holes on the {0 0 1} crystal facets. The {1 0 1} crystal facets serve as possible reservoirs of the photogenerated electrons [16,17]. In fact, density functional theory (DFT) calculations have predicted that the conduction band potential of the anatase (1 0 1) surface is slightly lower than that of the anatase (0 0 1) surface [18]. Furthermore, the

* Corresponding author at: Institute of Materials Science, NCSR "Demokritos", 153 10 Ag. Paraskevi, Attikis, Greece. Tel.: +30 210 650 3343; fax: +30 210 651 9430.
E-mail address: trapalis@ims.demokritos.gr (C. Trapalis).

0926-3373/$ – see front matter © 2013 Elsevier B.V. All rights reserved.
http://dx.doi.org/10.1016/j.apcatb.2013.06.009

exposed {1 0 1} crystal facets yield a highly reactive surface for the reduction of O_2 molecules to superoxide radicals [19]. This directional flow of the photogenerated charge carriers towards these specific crystal facets improves the reaction efficiency and selectivity of the photocatalyst. Moreover, dissociative water adsorption on the {0 0 1} crystal facets and molecular water adsorption on the {1 0 1} crystal facets have also been found in many theoretical studies [20–23]. More specifically, the structure and energetics of water adsorption on the anatase TiO_2 (1 0 1) and (0 0 1) surfaces at various coverages have been studied using density functional theory (DFT) calculations. It was shown that the molecular water adsorption is favoured on the (1 0 1) surface. The greater stability of the molecular state can be related to the presence of 2 H bonds between the hydrogens of the adsorbed molecule and two bridging surface oxygens. Instead, for the {1 0 1} facets, water molecules are found to be adsorbed dissociatively. More specifically, for temperatures above 230 K, only dissociated water in the form of hydroxyl groups are adsorbed on the {0 0 1} facets of the anatase crystal. The hydroxylation is suggested to occur on the 4-fold-coordinated Ti atoms located on the ridges of (4X1) reconstructed surface.

In this study we report the tunable photocatalytic selectivity of the TiO_2 anatase nanoplates according each time to the dominant exposed crystal facets. The photocatalytic evaluation of the nanoplates was investigated with the application of two different prominent air pollutants, the NO gas as an inorganic air pollutant and acetaldehyde as an organic air pollutant. The TiO_2 anatase nanocrystals were fabricated with a solvothermal method using Teflon-lined autoclaves. Two different surface modifications were applied in order to remove the adsorbed fluoride ions that were used in order to enhance the formation of the (0 0 1) surface of the anatase crystal. The first surface modification was by calcining the samples up to 600 °C. This process resulted in altering the structure of the crystal reaching its equilibrium state by expanding the stable {1 0 1} crystal facets and simultaneously shrinking the unstable {0 0 1} crystal facets. Whereas with the second surface modification the large percentage of the exposed {0 0 1} crystal facets of the anatase crystal, which were obtained by the solvothermal method, were maintained by washing the as-prepared products with a NaOH aqueous solution removing the adsorbed fluoride ions on the {0 0 1} crystal facets.

2. Experimental

2.1. Synthesis of TiO_2 anatase samples

TiO_2 anatase nanoplates with exposed {0 0 1} crystal facets were prepared using a solvothermal method. In a typical synthesis for TiO_2 anatase nanoplates, 3 mmol of titanium isopropoxide [$Ti(C_3H_7O)_4$] from Alfa Aesar Chemicals were dissolved into 50 mL of absolute ethanol from Merck under vigorous stirring at room temperature. 0.6 mL (0.03 mol) hydrofluoric acid (HF 40%) from Merck were added into the ethanol solution as a capping agent. Then the solution was poured into a 60 mL Teflon-lined autoclave until 80% of its volume was filled and was placed into the oven for 24 h at 180 °C. The as-synthesized powder product was collected through centrifugation of the solution. In order to obtain fluoride free TiO_2 anatase nanoplates, with no adsorbed fluoride atoms on their {0 0 1} crystal facets, two different surface modification procedures were applied. In the first surface modification the collected powder product was washed 3 times with distilled water and then dried in a furnace at 70 °C overnight. Then the as-prepared powder product was calcined in static air in a Muffle furnace for 90 min at 600 °C with a ramping rate of 5 °C/min and finally cooled to room temperature. In the second surface modification the collected reaction product was dispersed in 50 mL of 5 M NaOH aqueous solution and stirred for approximately 30 min. Then the dispersion was centrifugated and washed several times until the pH reached 7 and dried in a furnace at 70 °C overnight.

2.2. Characterization techniques

Differential scanning calorimetry (DSC) and thermogravimetry (TG) measurements were performed using NETZSCH equipment model STA 449C. The sample with a weight of ~14 mg was placed in alumina crucible and heated in air flow (30 mL/min) from room temperature up to 650 °C. The heating rate applied was 5 °C/min. The differential thermogravimetric (DTG) analysis was obtained by differentiation of corresponding TG curves, using the NETZSCH SOFTWARE FOR THERMAL ANALYSIS (Version 3.6), while the peak separation of the DTG curves was performed using NETZSCH SEPARATION OF PEAKS software (SW/PKS/650.01A). Chemical analysis of the TiO_2 anatase nanoplates were carried out with X-ray photoelectron spectroscopy (XPS) in an ultra-high vacuum VG ESCALAB 210 electron spectrometer equipped with a multichannel detector. The spectra was excited using Mg Kα (1253.6 eV) radiation (operated at 200 W) of a twin anode in the constant analyzer energy mode with pass energy of 30 eV. All the binding energies were referred to the C 1s peak at 284.8 eV and to the O 1s peak at 530.2 eV of the surface adventitious carbon and oxygen respectively. The crystalline phase of the TiO_2 anatase nanoplates was investigated by X-ray diffractometry (SIEMENS D500 diffractometer) using CuKα radiation. The measurements were performed using the following combination of slits: 1.0°/1.0°/1.0° as aperture diaphragms, 0.15° as detector diaphragm, and 0.15° as diffracted beam monochromator diaphragm. The measured 2θ range between 20° and 90° was scanned in steps of 0.03°/5 s. The accelerating voltage and applied current were 40 kV and 35 mA, correspondingly. The identification of the patterns was done with the cards of the International Centre for Diffraction Data. The shape and the crystal structure were observed with a transmission electron microscope (Philips CM20) operated at 200 kV and equipped with a Gatan GIF200 image filter. The TEM specimens of the TiO_2 anatase structures were prepared by direct deposition on a carbon coated Cu TEM grid. The Brunauer–Emmet–Teller (BET) surface area of the TiO_2 anatase nanoplates were analyzed by nitrogen adsorption using a Micrometrics FlowSorb II 2300 nitrogen adsorption apparatus. UV–vis diffuse reflectance spectra of all samples were obtained from the dry-pressed film samples using a UV–vis spectrometer (UV-2100, Shimadzu, Japan) with an integrating sphere attachment for their reflectance in the wavelength range 200–900 nm. $BaSO_4$ was used as a reflectance standard. The widths of the effective band gap of the samples were determined using Kubelka–Munk phenomenological theory.

2.3. Evaluation of the photocatalytic activity

The photocatalytic activity of the TiO_2 anatase nanoplates was studied in the oxidation of the NO gas following the ISO standard ISO/DIS 22197-1 [24] and in the acetaldehyde gas decomposition following the ISO standard ISO/DIS 22197-2 [25]. The as-prepared samples were pressed in sample holders with an apparent surface area of 20 cm^2 and then were pre-illuminated under a UV-A lamp with a light irradiance of 10 W/m^2 for three days in order to remove all possible organic residual compounds from the sample's surfaces. After the pre-illumination period the sample holders containing the TiO_2 powders were placed into the flow-type photoreactor with their surface parallel to an optical quartz window and were illuminated by UV-A radiation. The sample holders were separated from the window by a 5 mm thick air layer. The test gas passed only through the space between the sample holder and the window. The reactor is fabricated from materials that adsorb minimal NO or

acetaldehyde gas and withstand irradiation of near-UV light. Before the reaction, the catalyst was exposed to the pollutant containing air stream with no illumination until dark adsorption equilibrium was reached. Afterwards the illumination was switched on. The TiO_2 anatase nanoplates were exposed to model air containing 1 ppm nitric oxide (NO) or acetaldehyde (CH_3CHO). The photocatalyst adsorbs and oxidizes the NO to NO_2 and NO_3^- on its surface. In the case of the acetaldehyde it is also adsorbed on the photocatalyst surface and then decomposed. The performance of the photocatalyst is determined by the amount of the net removal of the nitrogen oxide (NO) and of the acetaldehyde. The adsorption and desorption of the NO gas on the surface of the photocatalyst was evaluated by monitoring the concentration of the gas in the dark. Pollutants and reaction products were analyzed on-line. In the case of NO oxidation a nitrogen oxides (NO_x) APNA-370 HORIBA analyzer was used. For acetaldehyde decomposition measurements a Syntech Spectras GC955 series 600 C6–C10 analyzer was applied. The photocatalytic activity of the samples was evaluated under UV-A light illumination with irradiance of 10 W/m^2 for 60 min. The photonic efficiency ζ (%) of the TiO_2 anatase nanoplates for the NO oxidation/acetaldehyde decomposition was calculated using the following equation:

$$\zeta = \frac{n_{\text{degraded molecules}}}{n_{\text{available photons}}} = \frac{\int_{t_0}^{t_1} AX[\text{ppm}]\,dt}{q_{n,p}T} \times 100\% \quad (1)$$

where t_0 is the time moment when UV-A light was switched on, t_1 is the time moment at the end of the illumination, T is determined by equation $T = t_1 - t_0$, A is the coefficient taken as a product of the gas flow value (3 L min^{-1} for NO and 1 L min^{-1} for acetaldehyde) and of the value 10^{-6} expressed in mol s^{-1} ($A = 2.08 \times 10^{-9}$ mol s^{-1} for NO and $A = 0.69 \times 10^{-9}$ mol s^{-1} for acetaldehyde), X (taken in ppm) is either the difference between the initial NO/NO_x concentration (~1 ppm) and the monitored NO/NO_x concentration or the directly monitored NO_2 concentration. In the case of the acetaldehyde it is the difference between the initial acetaldehyde concentration (~1 ppm) and the monitored acetaldehyde concentration. Lastly, $q_{n,p}$ is the photon flux of the samples' surface S (expressed in mol s^{-1}):

The photon flux of the sample's surface (mol s^{-1}) can be calculated as follows:

$$q_{n,p} = \frac{E\lambda S}{N_A hc} \quad (2)$$

where E is the irradiance (W/m^2), S is the apparent surface area (m^2), λ is the wavelength (m), N_A is the Avogadro constant (mol^{-1}), h is Plank's constant (J s) and c is the speed of light (m/s).

The rate of the gas flow, with 50% relative humidity, into the flow-type photoreactor was 3 L min^{-1} for the NO gas and 1 L min^{-1} for the acetaldehyde gas. The photonic efficiency of the monitored NO, NO_2, NO_x, acetaldehyde gases was calculated at the end of the illuminating period of time. The photocatalytic activity of Evonik Degussa P25 was also measured as a reference.

3. Results and discussion

3.1. TG, DTG, DSC analysis

Fig. 1 shows the TG, DTG and DSC curves of the TiO_2 anatase as prepared nanoplates which were used in order to study the thermal behaviour and to determine the temperature that the volatile compounds are removed from the sample. The TG analysis shows that mass loss of the sample, occurs up to 650 °C. More specifically the mass loss occurs mainly in three steps. The moisture is removed in the first step up to about 100 °C, while the other two steps were not well distinguished ones. According to the deconvolution of the DTG curve, the second step takes place from ~160 °C

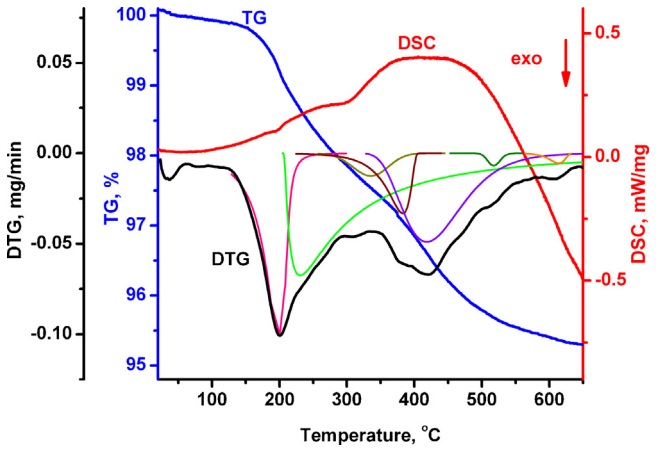

Fig. 1. TG and DSC curves, as well as the deconvolution of the DTG curves of the as-prepared TiO_2 anatase nanoplates.

(onset temperature) to ~370 °C (endset temperature), with a mass loss of 2.88%, and is attributed to the removal of enclaved water and other volatile compounds between the aggregated nanoplates. The second step is consisted from two stages indicating two different kind of enclaved water. The very broad tail at high temperatures of the second stage may indicate the existence of the adsorbed water molecules between parallel orientated nanoplates. The third step takes place between ~290 °C (onset temperature) and ~630 °C (endset temperature), with a mass loss of 1.71%, and is mainly attributed to the dehydroxylation process, according to the reaction:

$$TiO_{2-x}(OH)_{2x} \rightarrow TiO_2 + xH_2O \quad (3)$$

This step is consisted from five stages. In the DSC curve (Fig. 1), a strong exothermic tendency is observed between ~450 °C and 650 °C due to the crystallization phenomena. In this temperature range on the deconvoluted DTG curve two small peaks are observed at 517 °C and 614 °C which are attributed to the fluorine removal.

3.2. XPS analysis

In Fig. 2(a) XPS survey spectra of the TiO_2 anatase as-prepared, calcined and washed nanoplates is presented. As can be observed

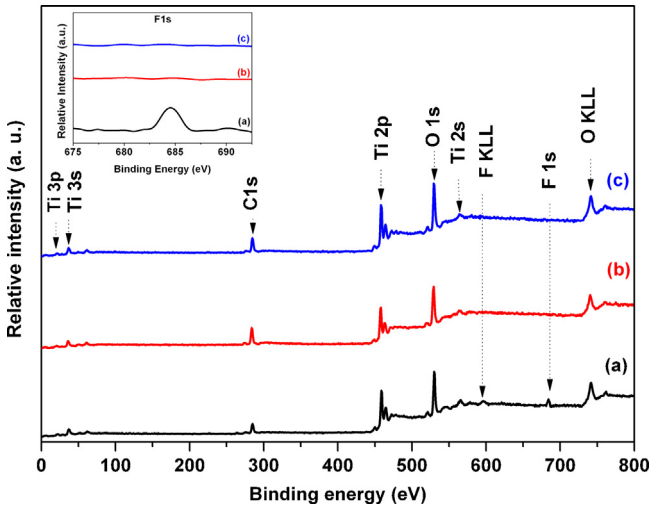

Fig. 2. XPS survey spectra and in the insert the high-resolution XPS spectrum of F 1s, of the TiO_2 anatase as-prepared nanoplates (a), calcined nanoplates (b), and washed nanoplates (c).

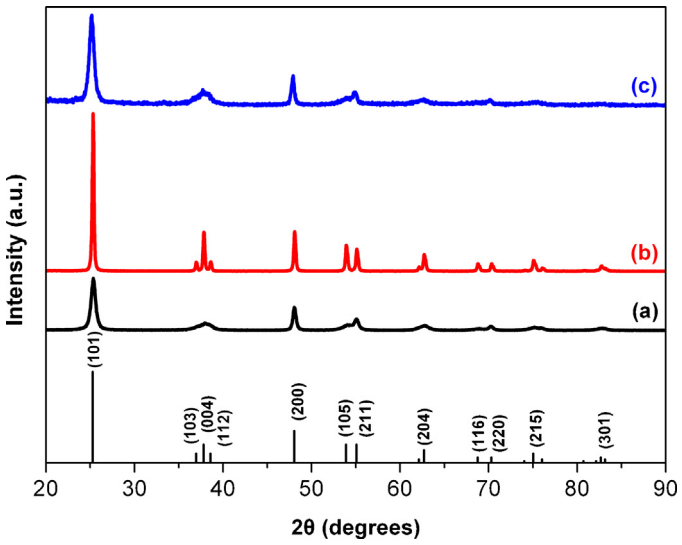

Fig. 3. XRD patterns of the TiO_2 anatase as-prepared nanoplates (a), calcined nanoplates (b), and washed nanoplates (c).

all samples have sharp photoelectron peaks at binding energies of 458 (Ti 2p) and 530 eV (O 1s). Another sharp photoelectron peak appears in all samples at binding energy 285 eV (C 1s) because of the contamination of the XPS instrument itself [26]. Moreover two peaks appear in the as-prepared nanoplates that refer to binding energies of 685 (F 1s) and 596 (FKKL). According to the literature [27–32] the fluoride binding energy peak originates from surface fluoride (≡Ti—F) formed by ligand exchange between fluoride anions (F^-) and surface hydroxyl groups [33]. The appearance of this specific peak indicates that the surface fluorination of TiO_2 readily takes place in an acidic hydrothermal environment. The disappearance of these peaks in the spectra of calcined and washed TiO_2 anatase nanoplates (Fig. 2(b and c) insert) indicates that the adsorbed fluoride atoms on the {0 0 1} crystal facets were entirely removed during their surface modifications either with calcination at 600 °C or with washing with a NaOH aqueous solution.

3.3. Phase observations

The XRD patterns of the calcined and washed TiO_2 nanoplates as well as those of the as-prepared nanoplates are presented in Fig. 3. It can be seen that the crystalline phase is anatase [JSPDS No. 021-1272 card] without any impurities of the remaining precursor used each time or the formation of another phase such as rutile or brookite. Certain Bragg peaks of the as-prepared TiO_2 nanoplates (Fig. 3(a)) are broad due to the anisotropic growth of the nanoplates along the *c*-axis of the anatase lattice [27,34,35]. This indicates that the (0 0 1) surface of the TiO_2 anatase crystal is larger than the (1 0 1) surface. Moreover, the Bragg peaks of the calcined TiO_2 anatase nanoplates (Fig. 3(b)) are narrow which is attributed to well defined crystals randomly oriented [36]. This implies that the calcined TiO_2 anatase nanoplates are larger in dimension than the washed ones and also that the anisotropic growth of the TiO_2 anatase nanoplates no longer exists after their calcination due to the expansion of the (1 0 1) surface, reaching this way the equilibrium state of the anatase crystal. The XRD diffraction diagram for the washed TiO_2 anatase nanoplates (Fig. 3(c)) have the same broadening for some Bragg peaks as the as-prepared ones. This implies that the shape of the nanoplates has been preserved after their surface modification with NaOH.

Table 1
Surface area of the studied TiO_2 anatase samples and percentage of their exposed {0 0 1} and {1 0 1} facets.

Sample	S_{BET} (m^2/g)	Percentage of exposed {1 0 1} facets (%)	Percentage of exposed {0 0 1} facets (%)
Agglomerates	66.48	68.6	31.4
Washed nanoplates	90.21	46.3	53.7

3.4. Morphological observations and BET surface areas

The TEM micrographs of the calcined and washed TiO_2 anatase nanoplates are presented in Figs. 4 and 5. It is obvious that the calcined nanoplates have larger dimensions than the washed nanoplates. This observation comes also in agreement with the XRD patterns. More specifically, the large square surface areas of the nanoplates are the {0 0 1} crystal facets and the small isosceles trapezoidal surfaces are the {1 0 1} crystal facets. The interfacial angles between two parallel and other surrounding faces is 68.3° which is the angle between the {0 0 1} and the {1 0 1} crystal facets (Fig. 4(b)). The side length of the calcined nanoplates is ~60 nm and their thickness is ~40 nm (Fig. 4(b)). As for the washed nanoplates the side length is ~40 nm and the thickness is ~6 nm (Fig. 5(b)). Furthermore, in a previous study the Rietveld method using the FullProf programme was applied for the analysis of the as prepared and calcined nanoplates. This study gave that the broadening of Bragg peaks for the calcined nanoplates is representative of instrument resolution and through this analysis the full width at half maximum (FWHM) parameters for instrument resolution function were obtained. FullProf programme calculations for the as-prepared nanoplates gave that the shortest apparent size was 6.1 nm and the longest was 40 nm [27]. These dimensions of the as-prepared nanoplates come in agreement also for the washed nanoplates according to the previously mentioned TEM analysis. This implies that after the calcination of the samples the {1 0 1} crystal facets of the nanoplates become almost 7 times larger and the {0 0 1} crystal facets become 1.5 times shorter than the washed ones. These observed changes are caused by the heat treatment of the nanoplates where the anatase crystal tends to reach its equilibrium state with the expansion of the energetically favoured {1 0 1} crystal facets (0.44 J/m^2) and the shrinkage of the relative higher energy {0 0 1} crystal facets (0.90 J/m^2). The percentage of the dominant {0 0 1} and {1 0 1} facets were calculated from the formula:

$$A = \frac{S_S}{S_L} \tag{4}$$

$$S_{\{001\}} = 1 - \left(2 - \frac{A}{\tan\varphi}\right)\frac{A}{\sin\varphi} \tag{5}$$

$$P_{\{001\}} = \frac{S_{\{001\}}}{S_{\{001\}} + S_{\{101\}}} \times 100\% \tag{6}$$

$$P_{\{101\}} = 100 - P_{\{001\}} \tag{7}$$

where S_S, S_L are the shortest and longest apparent size of the nanoplate respectively, φ is the angle between the {0 0 1} and the {1 0 1} crystal facets and is equal to 68.3° and $S_{\{001\}}$, $S_{\{101\}}$ are the areas of all {0 0 1} and {1 0 1} facets, correspondingly, of the nanoplates. For this study the percentage of the exposed {0 0 1} facets for the washed nanoplates was 68.6% and for the calcined nanoplates was 46.3%.

Table 1 shows the BET surface areas for the calcined and washed TiO_2 anatase nanoplates as well as the percentage of their exposed {0 0 1} and {1 0 1} facets. The nanoplates that have been calcined have a smaller specific surface area than the washed ones as has

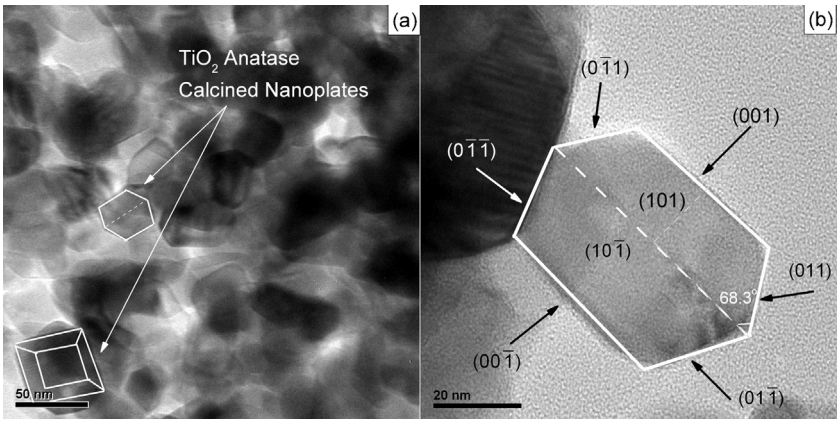

Fig. 4. TEM micrographs of the TiO_2 anatase calcined nanoplates.

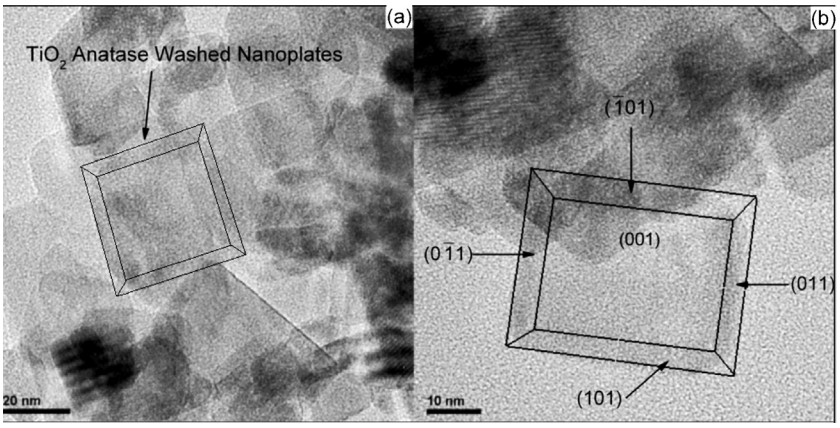

Fig. 5. TEM micrographs of the TiO_2 anatase washed nanoplates.

been already observed from the XRD patterns and the TEM micrographs. The reason for this decrease of the specific surface area for the calcined nanoplates is caused by the expansion of the {1 0 1} crystal facets reaching the equilibrium state, making the nanoplates larger in size.

3.5. UV–vis spectra

Fig. 5 shows the UV–vis diffuse reflectance and the absorbance spectra of the TiO_2 anatase calcined and washed nanoplates. The determination of the band gap of the samples was evaluated using the Kubelka-Munk method based on the diffuse reflectance spectra [37]. The $(F(R)E)^{1/2}$ versus E (eV) plots of the samples are presented in Fig. 6, where $F(R) = (1 - R)/2R$. As can be seen all samples absorb around 400 nm due to the band gap absorption of anatase TiO_2, which is ~3.2 eV. More specifically, the calcined nanoplates have an energy gap at 3.19 eV (Fig. 6(a)) and the washed nanoplates at 3.13 eV (Fig. 6(b)).

3.6. Photocatalytic activity

The photocatalytic activity of the calcined and washed TiO_2 anatase nanoplates was evaluated by oxidizing the NO gas as well as decomposing the acetaldehyde gas. In general the photocatalyst is activated by light, in the case of TiO_2 by UV-A irradiation, forming this way an electron and hole pair (e^-/h^+):

$$TiO_2 \xrightarrow{+h\nu} h^+ + e^- \quad (8)$$

The electron that has migrated to the {1 0 1} crystal facets of the TiO_2 anatase nanoplates [16,17] reacts with the favourably adsorbed O_2 [38] on these specific facets forming superoxide anions (O_2^-):

$$e^- + O_2 \rightarrow O_2^- \quad (9)$$

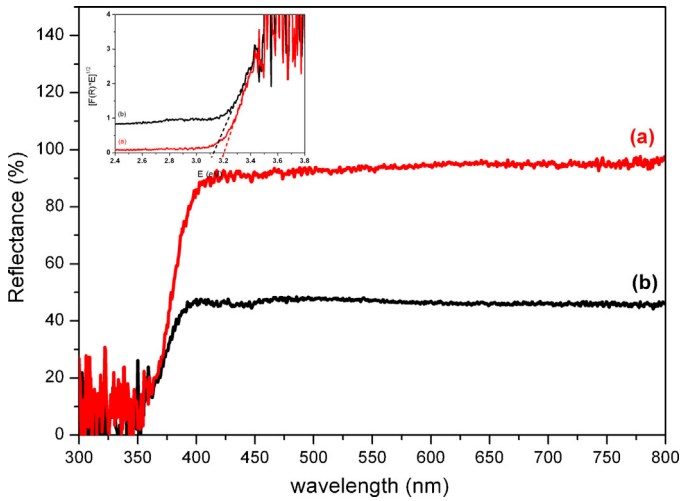

Fig. 6. UV–vis diffuse reflectance spectra and in the insert absorption spectra of the TiO_2 anatase calcined nanoplates (a) and washed nanoplates (b).

The superoxide anion O_2^- is a base and will form HO_2 radicals with traces of water that is originated from the humidity of the air flow [39–42]. The HO_2 may recombine to give H_2O_2:

$$2HO_2 \rightarrow H_2O_2 + O_2 \quad (10)$$

or may react with the NO gas, which is adsorbed on the {1 0 1} crystal facets of the TiO_2 anatase nanoplates, forming NO_2 and a hydroxyl radical [38,43]:

$$HO_2 + NO \rightarrow NO_2 \quad (11)$$

The products from the above reaction can further react to the end product which is nitric acid (HNO_3):

$$NO_2 + OH \rightarrow HNO_3 \quad (12)$$

All nitrogen species (NO, NO_2) are photocatalytically oxidized leading to nitrate (NO_3^-) where as O_2 is photochemically reduced according to the following chemical reaction:

$$NO + NO_2 + O_2 + H_2O \xrightarrow{TiO_2+h\varpi} 2HNO_3 \quad (13)$$

Previous experimental studies have shown that no photocatalytic decomposition of the NO gas was observed in the absence of O_2, since no HO_2 was formed in nitrogen [43]. Furthermore, it has shown that the first order rate constants for photochemical reactions of NO and NO_2 with TiO_2 are independent of the type of mixture of nitrogen oxides. This means that there is no inhibition of the decomposition of one compound by the other under experimental conditions applied.

These photochemically oxidation reactions for the NO gas and the simultaneous reduction of the O_2 take place on the {1 0 1} crystal facets of the TiO_2 anatase nanoplates. It is known from previous research that the NO gas is preferably adsorbed on the {1 0 1} crystal facet of the anatase crystal. More specifically, the N···Ti bond distances between the NO-nitrogen atom and the surface-Ti atom for the adsorption of the NO on the (0 0 1) surface is 2.21 Å and for the (1 0 1) surface is 2.00 Å. Furthermore, it has also been proven that the NO_2 gas adsorbs weakly on the TiO_2 anatase (0 0 1) surface where as on the TiO_2 anatase (1 0 1) surface the adsorption is much stronger. According to theoretical studies the NO_2 adsorption on the (1 0 1) surface of the anatase crystal ($\Delta E_{ads} = -125.56$ kcal/mol) is the most stable adsorption and much stronger than the (0 0 1) surface adsorption, specifically by 117.32 kcal/mol. The bond distances between the NO_2-nitrogen atom and the surface-Ti atom (N···Ti) for the TiO_2 anatase (0 0 1) surface is 2.62 Å and for the (1 0 1) surface is 2.14 Å, shorter by 0.48 Å [38]. Moreover, the oxygen O_2 adsorption on the TiO_2 anatase (1 0 1) surface is the strongest adsorption with an adsorption energy of −107.27 kcal/mol and much stronger than the adsorption on the (0 0 1) surface, specifically by 98.08 kcal/mol. The O···Ti bond distances between the O_2-oxygen atom and the surface-Ti atom for the adsorption of O_2 on the TiO_2 anatase (0 0 1) surface is 2.74 Å and on the (1 0 1) surface is 1.97 Å.

From the above experimental results and theoretical calculations is expected the photocatalytic NO oxidation to be favoured for the TiO_2 anatase nanoplates with the exposed {1 0 1} crystal facets rather than the ones with the exposed {0 0 1} crystal facets.

Fig. 7 shows the concentration profiles of NO, NO_2 and NO_x gases over the TiO_2 anatase nanoplates. A simple adsorption and desorption of the NO gas (not due to photocatalysis) in the dark by the anatase nanoplates is observed (Fig. 7(a) and (b)). The net removal of the NO gas at the beginning of the illumination for the calcined nanoplates is higher in comparison to that of the washed nanoplates. This behaviour can be explained by the fact that the NO gas and the oxygen O_2 are preferably adsorbed on the {1 0 1} crystal facets of the TiO_2 anatase nanoplates leading to the photochemical oxidation of the NO forming nitrate as a final product while O_2 is

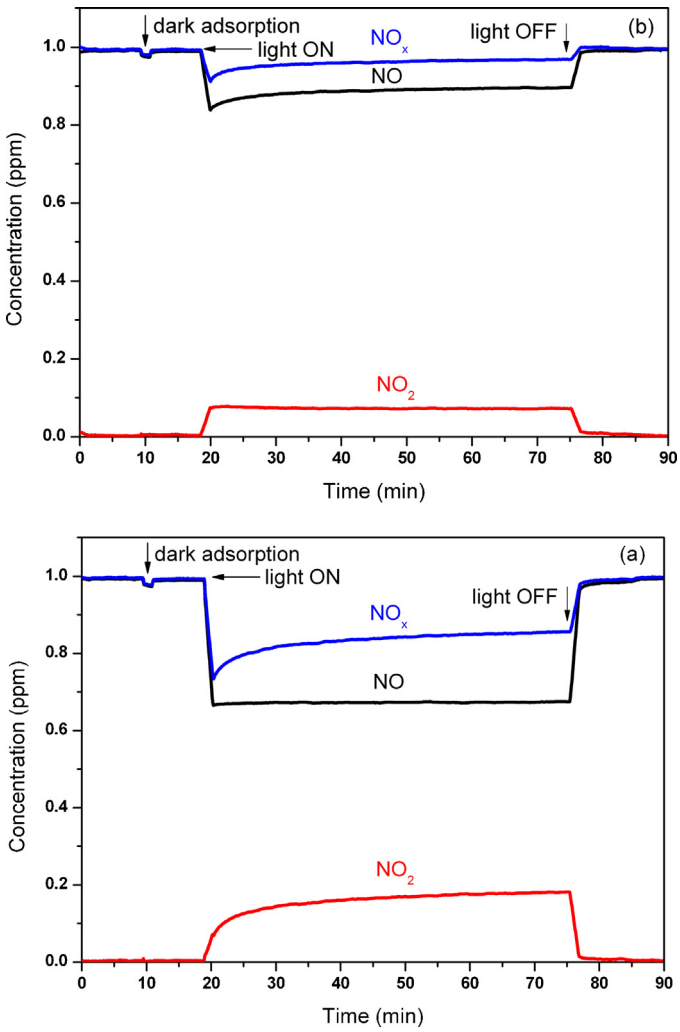

Fig. 7. Concentration profiles of NO, NO_2 and NO_x gases over the TiO_2 anatase calcined nanoplates (a) and washed nanoplates (b).

photochemically reduced. This behaviour can be explained by the fact that the calcined TiO_2 anatase nanoplates have larger {1 0 1} facets in comparison to the washed TiO_2 anatase nanoplates. Therefore larger amounts of the NO and NO_2 gases are adsorbed and then oxidized by the photocatalyst during the illumination period of time. The final product is NO_3^- which is in a solid state and thus blocks the catalyst surface, as a result the photocatalytic activity of the samples slightly decreases with time. This can be observed in Fig. 6 where the concentration of the NO gas at the beginning of the illumination time has rapidly decreased due to the clean surface of the photocatalyst and after a certain time it increases as NO_3^- products begin to block the oxidation sites of the photocatalyst.

The photogenerated holes that migrate to the {0 0 1} crystal facets of the TiO_2 anatase nanoplates react with the dissociated water molecules that are present on these particular facets creating active oxygen species, which have strong oxidative ability for many organic substances [44,45]:

$$H_2O + h^+ \rightarrow H^+ + OH \quad (14)$$

Previous studies have shown that acetaldehyde is photocatalytically degradated either by the OH radicals or by the photogenerated holes according to the following chemical reactions [46–49]:

$$CH_3CHO + OH \rightarrow CH_3CO + H_2O \quad (15)$$

$$CH_3CO + OH \rightarrow CH_3COOH \quad (16)$$

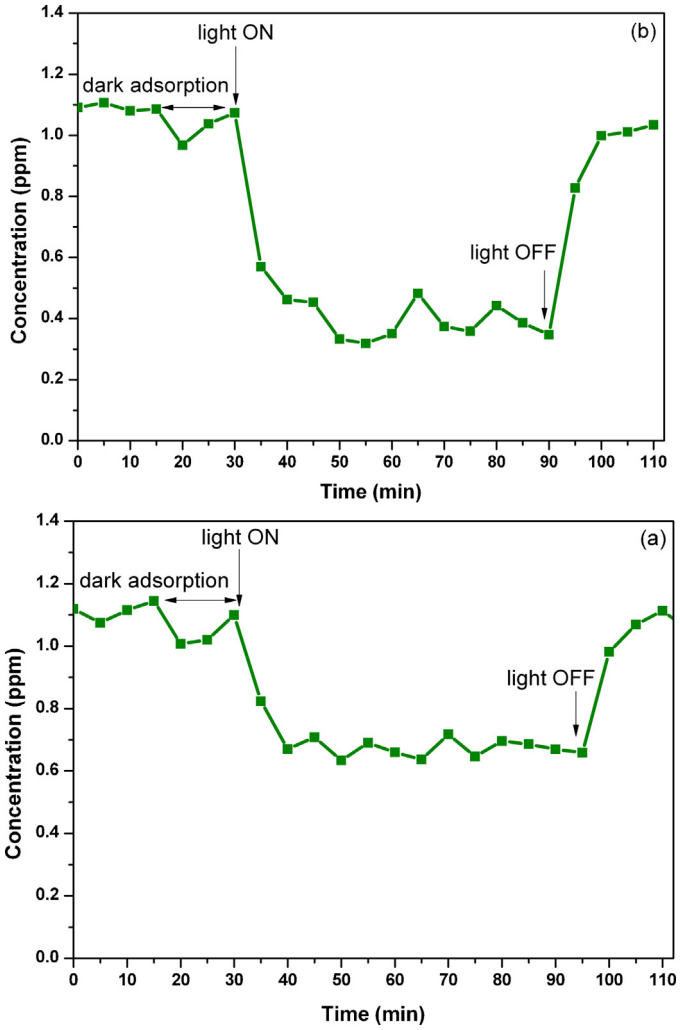

Fig. 8. Concentration profiles of acetaldehyde gas over the TiO_2 anatase calcined nanoplates (a) and washed nanoplates (b).

$$CH_3COOH + 2H_2O + 8h^+ \rightarrow 2CO_2 + 8H^+ \quad (17)$$

The previous stoichiometry is adopted with the assumption that the only radical species driving the photocatalytic degradation are the OH and the photogenerated holes. Acetic acid is formed which undergoes further oxidation to CO_2. However, it has been reported that when the number of the photogenerated holes on the TiO_2 surface is much larger than the number of the adsorbed acetaldehyde molecules, the proportion of direct oxidative conversion can be increases [47,48].

Fig. 8 shows the concentration profiles of acetaldehyde gases over the TiO_2 anatase nanoplates. A simple adsorption and desorption in the dark (not due to photocatalysis) of the acetaldehyde gas on the nanoplates is also observed (Fig. 8(a) and (b)). The net removal of the acetaldehyde gas during the illumination is higher for the washed nanoplates in comparison to the calcined nanoplates. This behaviour can be explained by the fact that the washed TiO_2 anatase nanoplates have larger {0 0 1} facets in comparison to the calcined nanoplates, as can be seen from the TEM micrographs, implying that more OH radicals are produced during the illumination period of time finally reacting with the acetaldehyde gas.

Fig. 9 shows the photonic efficiency of the studied nanoplates for NO oxidation and acetaldehyde decomposition. It can be seen that calcined nanoplates with larger {1 0 1} facets exhibited higher photonic efficiency for oxidation of NO to NO_2 and NOx removal

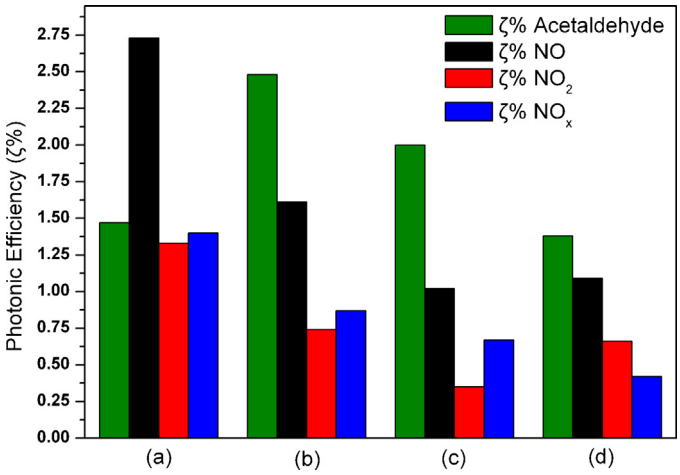

Fig. 9. Photonic efficiency of TiO_2 anatase calcined nanoplates (a), washed nanoplates (b) and P25 (c), for NO oxidation and acetaldehyde decomposition.

Table 2
Photonic efficiency of P25 and TiO_2 anatase samples for acetaldehyde decomposition and NO oxidation.

Samples	ζ % (mole/einstein)			
	Acetaldehyde	NO	NO_2	NO_x
Agglomerates	1.47	2.73	1.33	1.40
Washed nanoplates	2.36	1.02	0.35	0.63
As-prepared nanoplates	2.03	1.02	0.35	0.67
P25	1.38	1.09	0.66	0.43

in comparison to washed ones. The washed nanoplates preserving the initial crystal structure with larger {0 0 1} facets shows higher photonic efficiency for acetaldehyde decomposition. The photonic efficiency of Evonik Degussa P25 photocatalyst for oxidation of the same pollutants is also presented for comparison. The calculated photonic efficiencies of the investigated photocatalysts for acetaldehyde decomposition and NO oxidation are presented in Table 2.

From the above results and taking into consideration the photonic efficiencies of the TiO_2 anatase nanoplates and Evonik Degussa P25, a selective adsorption and photocatalytic oxidation-degradation of the inorganic–organic air pollutants is accomplished by altering the size of the exposed {1 0 1} and {0 0 1} crystal facets of the nanoplates.

4. Conclusions

TiO_2 anatase nanoplates were fabricated by a solvothermal method using hydrofluoric acid as a capping agent in order to fabricate pure and well defined anatase crystals with exposed {0 0 1} crystal facets. The removal of the adsorbed fluoride atoms was accomplished either by calcining the nanoplates or by washing them with a NaOH aqueous solution. These two different surface modifications of the TiO_2 anatase nanoplates influence their photocatalytic activity by creating a selective adsorption and photocatalysis of the air pollutant. More specifically, the calcination of the TiO_2 anatase nanoplates altered the structure of the TiO_2 anatase nanoplates by expanding the {1 0 1} crystal facet and simultaneously shrinking the {0 0 1} crystal facets. Contrary, washing the TiO_2 anatase nanoplates with a NaOH aqueous solution had no effect on the structure of the as-prepared nanoplates. The tunability of the structure of the TiO_2 anatase nanoplates lead to the selective adsorption of the air pollutant and their further photocatalytic oxidation or degradation. The calcined TiO_2 anatase nanoplates exhibited a favourably adsorption of the NO gas and

its photocatalytic oxidation. The washed TiO_2 anatase nanoplates exhibited a favourable adsorption of the acetaldehyde gas and its photocatalytic degradation. This observed selectivity of the adsorption and further photocatalytic oxidation-degradation of the air pollutant can be correlated with the different morphological structure of the TiO_2 anatase nanoplates. Further studies on this particular field need to be done.

Acknowledgements

This work was partially supported by the General Secretariat of Research and Technology of Greece under the project 09SYN-42-925, also by the Programme for the Promotion of the Exchange and Scientific Cooperation between Greece and Germany IKYDA 2010.

References

[1] C. Goss, S. Newsom, J. Schildcrout, L. Sheppard, J. Kaufman, American Journal of Respiratory and Critical Care Medicine 7 (2004) 816–821.
[2] J. Sunyer, European Respiratory Journal 5 (2001) 1024–1033.
[3] G.C. Allen, A. El-Turki, K.R. Hallam, D. McLaughlin, M. Stacey, British Corrosion Journal 35 (2000) 35–48.
[4] M.L. Bell, A. McDermott, S.L. Zeger, J.M. Samet, F. Dominici, Journal of the American Medical Association 292 (2004) 2372–2378.
[5] J.H. Seinfeld, S.N. Pandis, Atmospheric Chemistry and Physics – From Air Pollution to Climate Change, John Wiley and Sons, 1998.
[6] R.P. Wayne, Chemistry of Atmospheres, third ed., Oxford University Press, 2000.
[7] A. Fujishima, K. Honda, Nature 238 (1972) 37–38.
[8] M.R. Hoffmann, S.T. Martin, W. Choi, D.W. Bahnemann, Chemical Reviews 95 (1995) 69–96.
[9] J.G. Yu, J.J. Fan, K.L. Lv, Nanoscale 2 (2010) 2129–2144.
[10] D.Q. Zhang, G.S. Li, H.B. Wang, K.M. Chan, J.G. Yu, Crystal Growth & Design 10 (2010) 1130–1137.
[11] A. Feldhoff, C. Mendive, T. Bredow, D.W. Bahnemann, ChemPhysChem 8 (2007) 805–809.
[12] X.N. Wang, B.B. Huang, Z.Y. Wang, X.Y. Qin, X.Y. Zhang, Y. Dai, M.H. Whangbo, Chemistry - A European Journal 16 (2010) 7106–7109.
[13] A. Fujishima, X. Zhang, D.A. Tryk, Surface Science Reports 63 (2008) 82–515.
[14] X.Q. Gong, A. Selloni, Journal of Physical Chemistry B 109 (2005) 19560–19562.
[15] T. Ohno, K. Sarukawa, M. Matsumura, New Journal of Chemistry 26 (2002) 1167–1170.
[16] W.Q. Fang, X.Q. Gong, H.G. Yang, Journal of Physical Chemistry Letters 2 (2011) 725–734.
[17] T. Tachikawa, S. Yamashita, T. Majima, Journal of the American Chemical Society 133 (2011) 7197–7204.
[18] Y.F. Li, Z.P. Liu, L. Liu, W. Gao, Journal of the American Chemical Society 132 (2010) 13008–13015.
[19] N. Wu, J. Wang, D.N. Tafen, H. Wang, J.G. Zheng, J.P. Lewis, X. Liu, S.S. Leonard, A. Manivannan, Journal of the American Chemical Society 132 (2010) 6679–6685.
[20] A. Vittadini, A. Selloni, F.P. Rptzinger, M. Grätzel, Physical Review Letters 81 (1998) 2954–2957.
[21] A. Fahmi, C. Minot, Surface Science 304 (1994) 343–359.
[22] T. Bredow, K. Jug, Surface Science 327 (1995) 398–408.
[23] G.S. Herman, Z. Dohnálek, N. Ruzycki, U. Diebold, Journal of Physical Chemistry B 107 (2003) 2788–2795.
[24] ISO/DIS 22197-1. Fine ceramics (advanced ceramics, advanced technical ceramics). Test method for air-purification performance of semiconducting photocatalytic materials. Part 1. Removal of nitric oxide.
[25] BS ISO 22197-2. Fine ceramics (advanced ceramics, advanced technical ceramics). Test method for air-purification performance of semiconducting photocatalytic materials. Part 2. Removal of acetaldehyde.
[26] Y.L. Su, X.W. Zhang, M.H. Zhou, S. Han, L.C. Lei, Journal of Photochemistry and Photobiology A 194 (2008) 152–160.
[27] M.V. Sofianou, C. Trapalis, V. Psycharis, N. Boukos, T. Vaimakis, J.G. Yu, W.G. Wang, Environmental Science and Pollution Research 19 (2012) 3719–3726.
[28] Q.J. Xiang, K.L. Lv, J.G. Yu, Applied Catalysis B 96 (2010) 557–564.
[29] H. Park, W. Choi, Journal of Physical Chemistry B 108 (2004) 4086–4093.
[30] S.W. Liu, J.G. Yu, S. Mann, Journal of Physical Chemistry C 113 (2009) 10712–10717.
[31] S.W. Liu, J.G. Yu, M. Jaroniec, Journal of the American Chemical Society 132 (2010) 11914–11916.
[32] Q.J. Xiang, J.G. Yu, M. Jaroniec, Chemical Communications 47 (2011) 4532–4534.
[33] J.Y. Feng, M.C. Yin, Z.Q. Wang, S.C. Yan, L.J. Wan, Z.S. Li, Z.G. Zou, CrystEngComm 12 (2010) 3425–3429.
[34] C. Greaves, Journal of Applied Crystallography 18 (1985) 48–50.
[35] J.I. Langford, D. Louër, Journal of Applied Crystallography 15 (1982) 20–26.
[36] Th. E. Weirich, M. Winterer, S. Seifried, H. Hahn, H. Fuess, Ultramicroscopy 81 (2000) 263–270.
[37] E.L. Simmons, Journal of Modern Optics 19 (1972) 10845–10851.
[38] R. Wanbayor, V. Ruangpornivisuti, Journal of Molecular Structure: THEOCHEM 52 (2010) 103–108.
[39] C. Kormann, D.W. Bahnemann, M.R. Hoffmann, Environmental Science & Technology 22 (1988) 798–806.
[40] W. Kubo, T. Tatsuma, Analytical Sciences 20 (2004) 591–593.
[41] T. Hirakawal, Y. Nosaha, Journal of Physical Chemistry C 112 (2008) 15818–15823.
[42] K. Hashimoto, K. Wasada, N. Toukai, H. Kominami, Y. Kera, Journal of Photochemistry and Photobiology A 136 (2000) 103–109.
[43] S. Laufs, G. Burgeth, W. Duttlinger, R. Kurtenbach, M. Maban, C. Thomas, P. Wiesen, J. Kleffmann, Atmospheric Environment 44 (2010) 2341–2349.
[44] H. Einaga, A. Ogata, Journal of Hazardous Materials 164 (2009) 1236–1241.
[45] S. Matsuda, H. Hatano, Powder Technology 151 (2005) 61–67.
[46] T. Sano, N. Negishi, K. Uchino, J. Tanaka, S. Matsuzawa, K. Takeuchi, Journal of Photochemistry and Photobiology A 160 (2003) 93–98.
[47] Z.Y. Liu, X.T. Zhang, S.S. Nishimoto, T. Murakami, A. Fujishima, Environmental Science & Technology 42 (2008) 8547–8551.
[48] I. Sopyan, M. Watanabe, S. Murasawa, K. Hashimoto, A. Fujishima, Journal of Photochemistry and Photobiology A 98 (1996) 79–86.
[49] H.M. Hou, H. Miyafuji, S. Saka, Journal of Materials Science 41 (2006) 8295–8300.